QCD thermodynamics: an overview of recent progress

Francesca Cuteri[a,*]

[a]*Institut für Theoretische Physik, Goethe-Universität Frankfurt,*
Max-von-Laue-Straße 1, 60438 Frankfurt am Main, Germany

E-mail: cuteri@itp.uni-frankfurt.de

Recent results from lattice simulations of QCD at nonzero temperature and/or density and/or in presence of magnetic fields are reviewed. Progress in our understanding of the phases and boundaries in the phase diagram, as well as on the calculation of thermodynamic quantities with relevant phenomenological consequences are discussed.

---

*Speaker

1. Introduction

The theory of strong interactions, Quantum Chromodynamics (QCD), is one of the most fascinating physical theories. One of the many reasons is that it combines very solid mathematical foundations with a very rich phenomenology that describes a plethora of quite diverse phenomena and systems. The focus of this proceeding is on the thermodynamics of QCD that can give us a glimpse of the interior of neutron stars but can also serve as our standard toolbox in order to describe ongoing and future experiments of heavy ion collisions which aim towards the complete phase diagram of QCD and the search of the critical
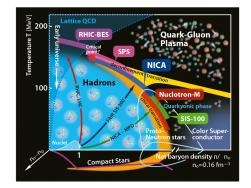

Figure 1: Sketch of the QCD phase diagram in the space of temperature, net baryon and net isospin density [1].

point of QCD. In this review we exclusively discuss the feverish progress of the past couple of years and we are not discussing the great experimental progress on the topic, for those, I refer the reader to the more appropriate literature. Nuclear material under conditions of extreme density, temperature, external fields can exhibit exotic properties such as color superconductivity and other features that one usually observes in condensed matter physics. But QCD at finite density is plagued by the infamous sign problem and in order to deal with it several algorithmic developments and new ideas have been proposed. A summary of all these new developments is presented in this review. For a recent review that goes beyond the scope of lattice gauge theory we refer the interested reader to [2].

2. Nonzero temperature

This section is devoted to applications at nonzero temperature in setups of QCD matter at vanishing chemical potentials and with no external electromagnetic fields. Contributions to this conference covering progress in this context are cited in the various subsections[1].

2.1 The thermal crossover/transition

We know for a fact that temperature triggers a change in the phase of QCD matter that is hadronic at low T and a plasma at high T (see Sec. 4.3). We also know that, while at nonzero densities i.e., nonzero chemical potentials we sometimes observe true phase transitions of first/second order, QCD matter at vanishing chemical potentials undergoes a continuous crossover at the physical point. However, for reasons that are only partly connected with simulation costs, lattice simulations have been often run at unphysical values of the quark masses, with results, on the order of the transition, that are condensed in Columbia-type plots with the light and strange quark masses on the axes. Many Columbia plots have been proposed that have common qualitative features, when it comes, for instance, to the heavy mass region and the location of the physical point in the crossover region, but

---

[1]In fact, there are some more [3, 4] along with results reported in other parallel sessions and in posters.

(a)   (b)
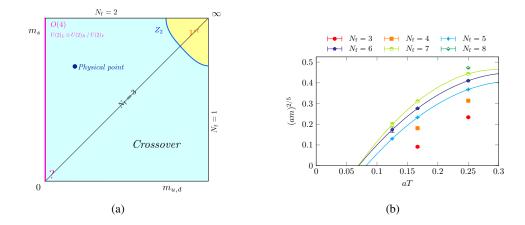
Figure 2: Figures from [5]. Fig. 2(a): The Columbia plot in the continuum. Fig. 2(b): Evidence of tricritical scaling for the chiral critical surface projected onto the (am, N_τ^{-1}) plane Fig. 2(b), (Every point represents a phase boundary with an implicitly tuned $\beta_c(am, N_f, N_\tau)$) showing that the regions of first-order transitions displayed in the bare parameter space of the standard staggered lattice theory (below the solid lines) are not continuously connected to the chiral limit in the continuum, and hence represent lattice artefacts.

that differ significantly when it comes to e.g. the location of the near chiral second order boundary across various lattice discretizations and for different numbers of flavors (see Table 1 in [6]).

Recent progress on our knowledge of the Columbia plot in the light mass region includes evidence based on expected tricritical scaling for the continuum chiral limit to feature second order transitions along the full y axis of the Columbia plot and beyond as displayed in Fig. 2. Recently simulations with Möbius domain wall fermions have also been run around the crossover at the physical point (with the input quark masses tuned by taking into account the residual mass due to a finite 5th dimension), and in order to establish the location of the second order critical point along the flavor symmetric line in the Columbia plot [7], with preliminary results (to be confirmed on larger volumes) indicating that the critical mass should be smaller than 3.7 MeV. As already mentioned, part of the reason for varying the quark masses away from their physical values was (and often still is) the cost of simulations along with the inconsistent results among discretizations that could, or sometimes could not, identify near chiral second order boundaries. As it was observed that first order regions become larger at nonzero imaginary chemical potentials, the community has been studying this setup with interesting recent results [8–12].

When it comes to the heavy mass region, the first order transition characterizing QCD in the quenched limit (and corresponding to the spontaneous breaking of the global center symmetry) is made weaker by the inclusion of heavy dynamical quarks until it turns into a smooth crossover at a Z_2 critical point. We, however, still lack continuum extrapolated results for the location of the Z_2 boundary and progress in this respect is being made. In Ref. [13], employing Wilson fermions and the hopping parameter expansion for $N_f \in \{1, 2, 3\}$ and on $N_\tau = 4$ lattices, the interesting observation was made that the distribution function of the real part of the Polyakov loop (from which an effective potential can be inferred, and the distance $\Delta\Omega$ between its minima can be extracted as in Fig. 3(a)) becomes consistent with Z_2 finite-size scaling on smaller aspect ratios LT than those needed to draw conclusions from studies of the corresponding kurtosis, and more
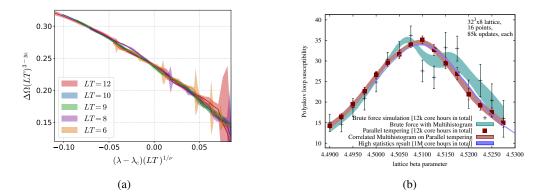
(a)

(b)

Figure 3: Fig. 3(a) shows the collapse plot over a wide range of aspect ratios LT and hoppings $\lambda \propto \kappa^4$ from the finite size scaling analysis of $\Delta\Omega$ (see text) around the critical temperature [13]. Fig. 3(b) displays the Polyakov loop susceptibility as a function of the coupling β in quenched QCD on a $32^3 \times 8$ lattice. Comparison among datasets shows the much better description of the high statistics result provided, resources being equal, by parallel tempering simulations [14].
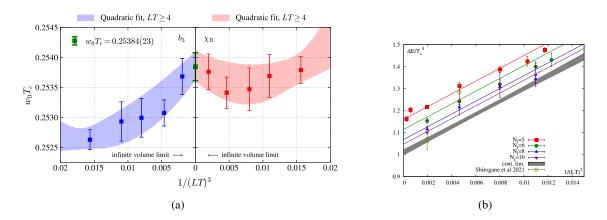

(a)

(b)

Figure 4: Figures from [14]. Fig. 4(a): Continuum extrapolated transition temperature $w_0 T_c$ and peak of the susceptibility as function of the inverse physical volume $(LT)^{-3}$. Fig. 4(b): Combined thermodynamic and continuum limit of the trace anomaly difference between the hot and cold phases.

recently [15] a method to take the effects of higher-order terms of the HPE up to a sufficiently high order to enable the extraction of reliable results for $N_\tau \geq 6$ was introduced. The bottleneck in studies that aim at locating the critical boundary in the heavy region seems to be the growth in autocorrelation times caused by supercritical slowing down for first order phase transitions that makes a rigorous finite size scaling very challenging. In Ref. [16] the two-flavor theory was simulated with staggered fermions on $N_\tau \in \{8, 10\}$ and to circumvent the issue of ever growing computational cost, an effective Ginzburg-Landau theory in the vicinity of the deconfinement critical point has been explored. Refs. [14, 17], instead, advocate the use of parallel tempering that allows swap updates between simultaneous calculations at different T. Advantages that have been measured in quenched QCD (see Fig. 3(b)), for which the first per-mille accurate results in thermodynamics were obtained with the critical temperature in the thermodynamic and continuum limit (see Fig. 4(a)), along with an accurate determination of the latent heat (see Fig. 4(b)).
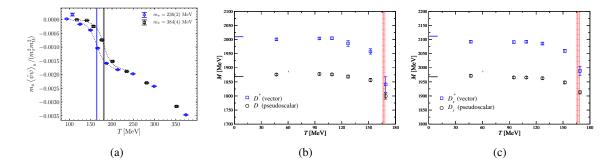
(a)   (b)   (c)

Figure 5: Fig. 5(a): The renormalised chiral condensate for $N_f = 2$ light quarks for the two available ensembles [18]. Vertical lines indicate the inflection points corresponding to pseudo-critical values of the temperature. Fig. 5(b): Temperature dependence of the groundstate masses in the hadronic phase, for D and D^* mesons [19]. The vertical band indicates the thermal transition, the horizontal stubs at $T = 0$, the PDG values. Fig. 5(c): Same as Fig. 5(b) for D_s and D_s^* [19].

2.2 Thermal effects on hadrons

Before the actual crossover/transition takes place one can look at how hadrons in their ground state masses, spectra and interquark potentials respond to temperature variations within the confined phase. These effects have been the focus of several investigations by the FASTSUM collaboration [18–23], that take advantage of dedicated newly generated "Generation 2L" ensembles. These are ensembles with anisotropic lattice spacings and with several temperatures simulated in a fixed-scale approach. Two different values of the pion mass are available. Results on fundamental thermodynamics observables are obtained such as the T-dependence of the renormalised chiral condensate where a 20 MeV shift in the pseudo critical temperature is identified comparing the two available pion masses (see Fig. 5(a)). Progress was made on the reconstruction of spectra of NRQCD bottomonia (η_b, Υ, χ_{b1}, h_b) [22] using the Backus-Gilbert method, and new results were obtained on the thermal interquark potential of bottomonium using the HAL QCD method with NRQCD quarks [23]. Moreover, the first systematic study throughout the hadronic phase on open charm D and D_s mesons was performed. Using the determined groundstate mass at the lowest temperature, the effect of rising temperature was investigated by analysing ratios of mesonic correlators [20, 21] (see Figs. 5(b) and 5(c)), without the need for further fitting or spectral reconstruction and temperature effects, and found to be at the percentage level.

2.3 From the hadronic to the QGP phase: correlators, screening masses, spectral functions

Raising the temperature further to enter the QGP phase, there is plenty of phenomenologically relevant (for instance for heavy ion collisions) observables that the community has (further) investigated over the past year. Starting, for instance, from the complex static potential at nonzero temperature. The real and imaginary parts of the static potential are connected respectively to the position Ω and effective width Γ/T of the dominant peak in the spectral function corresponding to Wilson line correlators in the Coulomb gauge, that can be reconstructed based on several fit *Ansätze* or Bayesian methods. Results [24] indicated a strong T dependence for the imaginary part of the potential as opposed to the approximate T-independence, and lack of screening, visible in the real
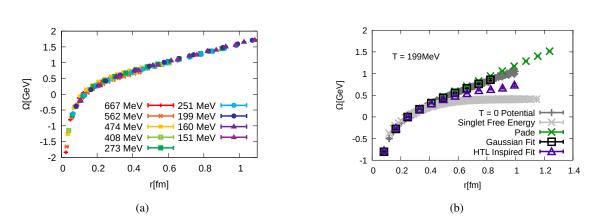
Figure 6: Figures from [24].Fig. 6(a): The peak position Ω as a function of separation distance, at different temperatures, as obtained from Padé interpolation for $N_\tau = 12$ lattices. Fig. 6(b): Comparison of Ω as a function of separation distances as obtained from different methods, for $T = 199$ MeV.

part of the potential. Newer results [25] were obtained on a new set of $N_f = 2 + 1$ HISQ ensembles with $T \in [127 - 354]$ Mev produced by the Hot QCD collaboration, with physical strange quark mass and light quark mass corresponding to a 310 MeV pion (corresponding to $m_l = m_s/5$) on very large ($96^3 \times N_\tau$) and much finer ($1/a = 7.1$ GeV) lattices as compared to the ones used in Ref. [24]. There remains the issue that the results extracted for Ω and Γ/T seem to strongly depend on the used reconstruction method, hence on the assumptions that the various methods rely on.

Preliminary results were obtained [26] also for the pseudoscalar charmonium and bottomonium correlation functions from physical clover-improved Wilson valence quarks on the same HISQ ensembles (specifically at $T = 251$ MeV). In the same study the perturbative spectral function in the pseudoscalar channel was then constructed by smoothly matching the thermal and vacuum parts.

Moving on to the thermal splitting of the vacuum pion mass into a lower pion quasiparticle mass and a higher pion screening mass, previous results [27] have been confirmed and extended [28, 29] based on the availability of a newer ensemble with $2 + 1$ clover improved fermions at physical quark masses and $T = 128$ MeV. A modified dispersion relation for the pion quasiparticle (also used to estimate the quark number susceptibility) is presented. The pion quasiparticle is found to be significantly lighter than the zero-temperature pion mass, despite the shorter corresponding static correlation length. As order parameter for chiral symmetry restoration, the difference of the vector- and axial-vector time-dependent correlators is considered and found to be reduced by a factor $\sim 2/3$ as compared to its vacuum counterpart.

Within this section it is also worth mentioning a strategy proposed recently to explore QCD up to the EW scale and beyond, that fits at this point, in light of the fact that its first application consisted in measurements of the flavor non-singlet meson screening masses in QCD with three flavors of massless quarks for $T \in [1 - 160]$ GeV. The huge temperature range is made accessible by a scale-setting strategy that exploits a non-perturbative, finite-volume, definition of the strong coupling constant to renormalize the theory, along with step scaling techniques. An extended comparison with perturbation theory becomes then possible. Fig. 7(a) illustrates the large relative corrections to the perturbative result even at the electroweak scale. Fig. 7(b) shows that the mass-difference
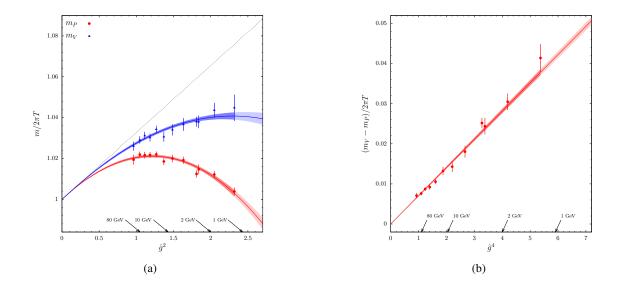
Figure 7: Figures from [30].Fig. 7(a): *T*-dependence of PS- and V- screening masses (normalized to their free value) compared to NLO-PT. Fig. 7(b): Splitting between V and PS screening masses.

between vector and pseudoscalar mass, due to higher order effects which cannot be not explained by the 1-loop perturbative calculation, which is non-negligible in the entire temperature range.

Still concerning light meson screening masses and to what extent their behavior can be explained in perturbation theory, there is a trend already measured on HISQ ensembles [31] that is likely signalling a change of dynamics and is neither compatible with the perturbative behavior, nor something that higher order corrections can accommodate. This is the change from roughly vertical to nearly horizontal *T*-dependence of the screening masses divided by *T*, within a narrow temperature range of $T \in [0.15 - 1]$ GeV (see Fig. 9 in [31]). This trend is brought [32] as additional evidence, along with previously observed multiplet patterns in Domain Wall simulations for $N_{\mathrm{f}} = 2$ for the emergent chiral spin symmetry discussed in Refs. [33, 34]. In a scenario with chiral spin symmetry at work there would be three temperature regimes with distinguishable symmetries in QCD with an intermediate, approximately SU(4)-symmetric, one featuring a dominance of color electric quark-gluon interactions before these too get screened at about $3T_c$ and the usual chiral symmetry gets recovered via a crossover. Moreover, on symmetry grounds and based on the behavior of screening masses, the chiral spin symmetric band would continue to finite baryon density and bend downwards (see Fig. 8). The nature of the effective degrees of freedom in the different regimes may be encoded in the pion spectral function, which is extracted via a newly proposed method [35] that applies to stable scalar particles in a heat bath and allows to circumvent the integral inversion by exploiting constraints imposed by field locality at nonzero T that lead to a representation of the spectral functions in terms of damping factors that can be fitted by spatial correlators on the lattice.

2.4 Transport properties

The spectral function associated with the 2-point correlator of the EM current at lightlike kinematics is the one we need to access if we want a measure of how brightly the QGP glows i.e., of the photon emissivity, which is very important for phenomenology to predict photon yields in
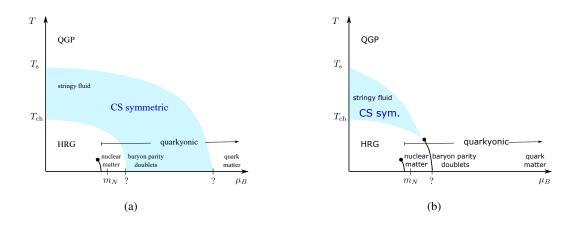
Figure 8: Figures from [34]. The QCD phase diagram with a chiral spin and SU(4)-symmetric band.
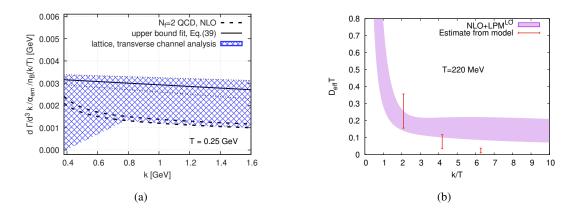

Figure 9: Fig. 9(a): The photon rate per unit volume of the QGP at $T \simeq 250$ MeV (hatched band) from [36]. Fig. 9(b): Effective diffusion coefficients, as obtained from various models, combined. Here the photon production rate is reexpressed in terms of the so-called effective diffusion coefficient $D_{\mathrm{eff}}(k) \equiv \frac{\rho_H(k,\vec{k})}{2\chi_q k}$.

HIC and it is what we need in the soft-photon regime to tell apart a weakly coupled from a strongly coupled plasma.

Recent results on the photon emissivity were obtained by two groups based on simulations employing two different fermion discretizations, but otherwise in similar lattice setups. In Ref. [36] the photon emissivity (along with the lepton-pair production rate) is computed based on continuum-extrapolated (Euclidean) time-dependent correlators with $N_{\mathrm{f}} = 2$ $O(a)$-improved Wilson fermions at $T \sim 1.2 T_{\mathrm{c}}$ and $m_\pi \sim 270$ MeV. Their final result for the photon emissivity is displayed in Fig. 9(a) as a hatched band. In Ref. [37], the photon production rate is extracted on $N_{\mathrm{f}} = 2 + 1$ flavor HISQ configurations with $m_l = m_s/5$ at a temperature of about $1.15 T_{pc}$ (220 MeV). Using for the spectral function two different *Ansätze* (a polynomial connected to the UV region consistent with the OPE expansion and a hydro-inspired spectral function) and the Backus-Gilbert method different results are obtained and combined in a final estimate (see Fig. 9(b)).

It remains true, for the above mentioned studies of the photon emissivity, that accessing the spectral function using Euclidean data is challenging due to the ill-posed nature of inverting the
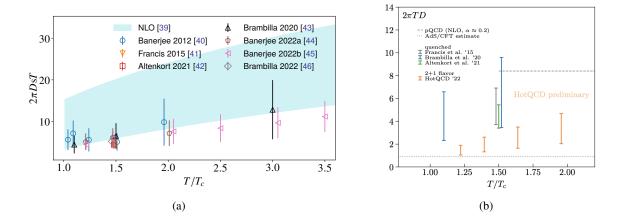
(a)   (b)

Figure 10: Fig. 10(a): Results for κ_E from [46] compared to other existing lattice results. Points at the same temperature are slightly shifted horizontally for better visibility. Figure source from [47]. Fig. 10(b) (from L. Altenkort's talk): first results in full QCD compared to quenched ones.

Laplace transform. In Ref. [38] the first results on implementing the proposal of directly computing the analytic continuation of the retarded correlator at fixed, vanishing virtuality of the photon via the calculation of the appropriate Euclidean correlator at imaginary spatial momentum is presented and tested on $N_f = 2$ $O(a)$-improved Wilson fermions configurations at $T \sim 250$ MeV.

Another very relevant, for phenomenology, question to ask about the hot QCD medium is how fast do heavy quarks thermalize in it. The answer to this question is encoded in three related transport coefficients that appear in the Langevin equations that describe this thermalization. These transport coefficients are related to Euclidean correlators of field strength tensor components in the heavy quark limit. The heavy quark diffusion coefficient (D, or D_s in Fig. 10), in particular, is encoded in the spectral functions of the chromo-electric and the chromo-magnetic correlators, of which the latter describes the T/M contribution. Recently these correlators have been studied [46, 47] at two different temperatures $T = 1.5T_c$ and $T = 10^4 T_c$ in the deconfined phase of the SU(3) gauge theory. Results (see Fig. 10(a)), in agreement with previous ones [44], show that the mass suppressed effects in the heavy quark diffusion coefficient are 20% for bottom quarks and 34% for charm quarks at $T = 1.5T_c$. The temperature dependence of the static quark diffusion coefficient has also more recently been analyzed up to $T \sim 3.5T_c$ [45] and for the first time measurements of this coefficient have been performed on $N_f = 2 + 1$ flavor HISQ configurations with $T \in [200 - 350]$~MeV (see Fig. 10(a)).

3. Nonzero EM fields or vorticity

With the quark gluon plasma coined as the most vortical and strongly magnetized plasma in nature, in many applications the community is pushing for improving our understanding of QCD in the relevant regimes. This section is devoted to the progress in this direction that has been reported at this conference.
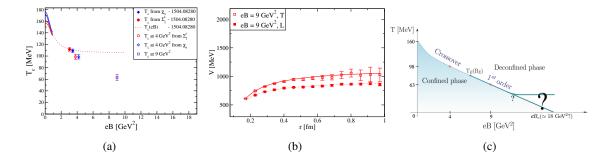
Figure 11: Figures from [48]. Fig. 11(a): Transition temperatures as a function of the external magnetic field intensity showing an unpredicted steady drop of T_c as a function of eB. Fig. 11(b): Static quark-antiquark potential for the transverse (T) and longitudinal (L) directions fitted to a purely Coulombic potential at $eB = 9\,\mathrm{GeV}^2$. Fig. 11(c): Updated sketch of the QCD phase diagram in an external magnetic field.
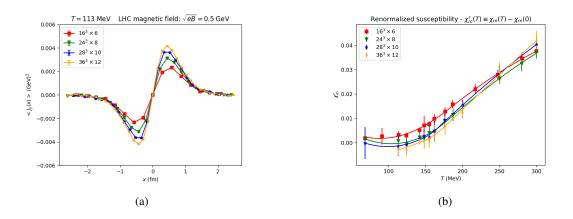

Figure 12: Figures from D. Valois' talk. Fig. 12(a): Bare electric current as a function of x at $T = 113$ MeV and LHC-like magnetic fields. Fig. 12(b): Renormalized magnetic susceptibility as a function of T.

3.1 Nonzero EM fields

The QCD phase diagram in the $T - B$ plane has been the subject of several recent investigations. An effective action describing the asymptotically strong magnetic field limit is an anisotropic pure gauge theory that has been simulated [49]. Results provided evidence for a first-order deconfinement phase transition in the limiting theory, implying the presence of a critical point in the $T - B$ QCD phase diagram. More recently [48, 50], evidence from lattice simulations of $N_f = 2 + 1$ stout-improved staggered quarks was found for a crossover at $eB = 4\mathrm{GeV}^2$, and a strong 1st order phase transition is, indeed, observed at $eB = 9\mathrm{GeV}^2$ (see Fig. 11(a)). Based on results for the static potential, the transition at these strong fields seems to be one from a strongly anisotropic confined phase to a completely deconfined one with zero string tension in all directions (see Fig. 11(b)). Moreover, the steady decrease of the critical temperature with B is what led to the cartoon of the phase diagram in Fig. 11(c) highlighting the existence of a critical endpoint and the fact that whether a transition driven by B only is possible, remains unclear.

As a first step towards a more realistic modeling of the complex heavy-ion collision scenario in lattice simulations inhomogeneous field backgrounds have been considered [51], lately, based on
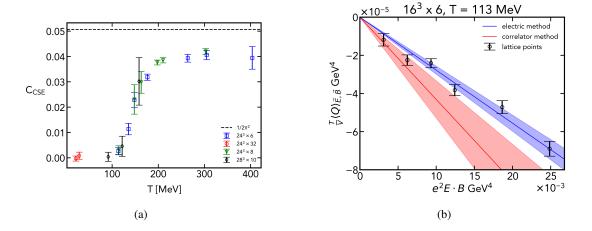
10

Figure 13: Fig. 13(a) (from [52]): C_{CSE} at physical quark masses for a wide range of temperatures and four different lattices. The black dashed line represents the analytical prediction for the free case with massless quarks. Fig. 13(b) (from [53]): $\langle Q_{\text{top}} \rangle$ as a function of $\vec{E} \cdot \vec{B}$.

a phenomenologically-inspired $1/\cosh^2$ Ansatz. Besides the impact of the inhomogeneity on the quark condensate and Polyakov loop the steady electric currents flowing in the system as a response to the inhomogeneous field are measured and used to extract the magnetic susceptibility of the QCD medium (see Fig. 12).

The interplay between quantum anomalies and electromagnetic fields leads to a series of non-dissipative transport effects in QCD, such as the chiral magnetic effect - generation of a vector current in the presence of a chiral imbalance and a magnetic field B - and the Chiral Separation Effect (CSE) - emergence of an axial current J^5 in the presence of finite density and a magnetic field B. The latter effect is being investigated [52] via lattice QCD simulations aimed at determining the CSE conductivity C_{CSE} and analyzing its dependence on the temperature T and the mass m of the quarks. To first order, the current is linear in the magnetic field (assumed to point in the z direction) and in the baryon chemical potential μ

$$J_3^5 = \sigma_{\text{CSE}} \, eB = C_{\text{CSE}} \, \mu \, eB + O(\mu^3) \tag{1}$$

with J_3^5 the z-component of the axial current. One can then measure the derivative of the CSE current with respect, e.g., to the baryon chemical potential

$$\left. \frac{\mathrm{d} \langle J_3^5 \rangle}{\mathrm{d}\mu} \right|_{\mu=0} = C_{\text{CSE}} \, eB \tag{2}$$

via simulations at $\mu = 0$, free of the sign problem. Based on this, the dependence of C_{CSE} on the temperature in the interacting case at physical quark masses was found (see Fig. 13(a)) to approach the free case prediction as expected at temperatures higher than T_c, and to go to zero at temperatures below T_c, which indicates that the CSE might be very suppressed at low T.

The introduction of non-orthogonal electric and magnetic fields in the QCD vacuum triggers a different effect consisting in the enhancement of the weight of topological sectors with a nonzero topological charge. For sufficiently weak fields, there is a linear response for the expectation value

11

of the topological charge, which has been confirmed [53] - via lattice simulations at physical masses, including background magnetic and (imaginary) electric fields - and related to the QCD correction to the axion-photon coupling. The direct coupling between axions and photons is of the form $g^0_{a\gamma\gamma} a F_{\mu\nu}\tilde{F}^{\mu\nu}/4 = g^0_{a\gamma\gamma} a \vec{E} \cdot \vec{B}$. After the QCD path integral, the QCD corrections to this term in the effective action can then be found as

$$g_{a\gamma\gamma} f_a = \left. \frac{T}{V} \frac{\partial^2}{\partial\theta\,\partial(\vec{E}\cdot\vec{B})} \ln Z \right|_{\theta=\vec{E}=\vec{B}=0} , \tag{3}$$

where Z includes constant background electromagnetic fields and a functional derivative with respect to the homogeneous axion field is traded for a derivative with respect to θ from the CP-odd θ-term in the QCD Lagrangian. Based on this relation two methods to extract the coupling, by computing one or two derivatives of the partition function (called the electric- and correlator method, respectively) are applied [53] (see Fig. 13(b)).

3.2 Vorticity

The (pseudo)critical temperature T_c in QCD changes as a result of relativistic rotations and, based on several phenomenological/effective models, a decreasing trend is to be expected. However, results from quenched simulations rather indicate that T_c in gluodynamics increases due to rotation. Over the past year the first lattice results for QCD with $N_f = 2$ dynamical clover-improved Wilson quarks at nonzero vorticity (with rotation introduced via an external gravitational field) have been obtained [54]. The system was simulated in a sign-problem free setup at nonzero imaginary angular velocity, and after performing the analytic continua-
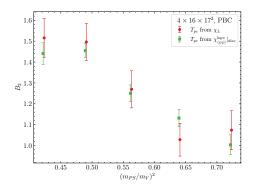

Figure 14: Figure from [54]. The coefficient B_2 in Eq. (4) for confinement-deconfinement and chiral crossovers as a function of $(m_{PS}/m_V)^2$.

tion to real angular velocity, T_c, as extracted both from the susceptibility of the averaged Polyakov loop and from the (disconnected) chiral susceptibility, was found to increase quadratically with angular velocity

$$\frac{T_{pc}(v)}{T_{pc}(0)} = 1 + B_2 v^2 , \tag{4}$$

(where $v \propto \Omega$, the angular velocity) with the coefficients of proportionality reported in Fig. 14. Dependence of the results on the pion mass was also analyzed and, for all considered values of the pion mass ($m_{PS}/m_V = 0.65,\ldots,0.85$), $B_2 > 0$ was obtained, i.e, T_c in rotating QCD was found, just like in SU(3) gluodynamics, to increase with rotation.

4. Nonzero density

This section is devoted to applications for which a nonzero density is considered. It is very well known that at nonzero baryon density standard Monte Carlo simulations are hindered by the complex
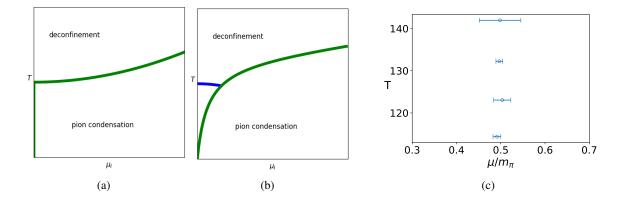
Figure 15: Figures from [61]. Figs. 15(a) and 15(b): Two possibilities for the phase diagram in the T-μ_I plane in the chiral limit. Fig. 15(c): Points on the pion condensation boundaries, from the $24^3 8$ lattices.

action, also known as sign problem, and that the community has developed several strategies either to infer properties in non-simulable domains from results of simulations in sign-problem-free setups, or to work out effective theories with a milder sign problem, or to employ complex Langevin simulations (see [55] and [56] for progress documented at this conference) or contour deformations (see [57] for progress documented at this conference). In the coming subsections studies that have been discussed at this conference are "classified", not based on the methods/approaches used, but rather based on the physics they aim at extracting.

4.1 The phase diagram

Lee-Yang theory is one of the most promising approaches to the study of phase transitions. Lee-Yang zeros are points in the complex plane of an external control parameter at which the partition function vanishes. In the thermodynamic limit, they approach the critical value on the real-axis, where a phase transition occurs. Recently, a new method has been proposed [58] to look for phase transitions in the QCD phase diagram at nonzero μ_B, which can be regarded as a combination of the Taylor expansion and the analytic continuation approaches. For any given observable the Taylor series coefficients at zero and purely imaginary chemical potentials are computed and then the Taylor series are merged by using multi-point Padé approximants. These can then be analytically continued to real μ_B. Moreover, information about the analytical structure of the observables can be obtained by studying the poles of the approximants. As a proof of concept of its reliability, the method was applied to the case of the two-dimensional Ising model [59]. Moreover, in QCD [60] (I) in the high temperature regime the LYE singularities associated to the Roberge-Weiss endpoint have been identified and shown to have the expected critical behaviour for a transition belonging to the 3d-Z(2) universality class, and (II) in the low temperature regime singularities were found that may be identified as the LYE singularities associated with either the chiral transition or the critical endpoint of QCD.

Coming to nonzero isospin density and the phase diagram in the T-μ_I plane, we know that at large enough isospin chemical potentials there is a Bose-Einstein condensation (BEC) phase, separated from the normal one by a phase transition. The location of the BEC line at physical quark masses is known. In the chiral limit it is known, according to chiral perturbation theory, that
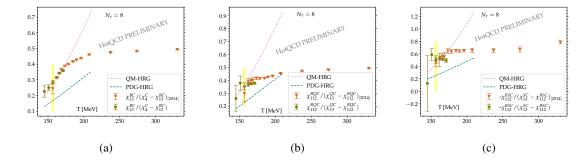
Figure 16: Figures from [62]. Ratios of baryonic to mesonic contribution to the partial charm pressure in the charm (Fig. 16(a)), electrically-charged charm (Fig. 16(b)), strange-charm (Fig. 16(c)) sectors.

condensation happens already at infinitesimally small isospin chemical potential at $T = 0$. The thermal chiral transition at zero density might then be affected, depending on the shape of the BEC boundary, by its proximity. As a first step towards the chiral limit, simulations of $N_{\rm f} = 2 + 1$ QCD at half the physical quark masses have been performed [61]. Results (at fixed lattice spacing) show that the vertical direction of the pion condensation line is preserved, at least up to $T \sim 142$ MeV, when going to smaller light quark masses (see Fig. 15(c)), hence pointing for the chiral limit to the scenario shown in Fig. 15(a) rather than to the one in Fig. 15(b).

4.2 Fluctuations of conserved charges

Ratios of cumulants of conserved net charge fluctuations are sensitive, in different phases of strong interaction matter, to the degrees of freedom that are carriers of the corresponding quantum numbers.

The nature of charmed degrees of freedom as well as details of the charm hadron spectrum in the vicinity of the QCD chiral crossover region has been probed [64] by analyzing appropriate ratios of these cumulants. A few years later the same type of analysis [62] can capitalize on the availability of more (at higher T and at the physical point) and way larger HISQ $N_{\rm f} = 2 + 1$ gauge configuration ensembles with the charm sector treated in the quenched approximation.

Results point to (I) the dissociation of open charm hadrons and the emergence of deconfined charm states setting in right after the chiral crossover transition, and, possibly, (II) yet unobserved baryonic states in the open-charm sector that contribute to the thermodynamics in the crossover region (see Fig. 16).
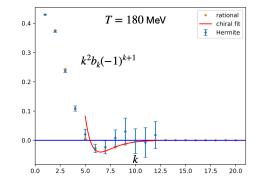

Figure 17: Fourier coefficients $b_k(T)$ of the net baryon number density $\mathrm{Im}[\chi_1^B]$ as a function of the frequency k at $T = 180$ MeV from [63]. A Fit to the expected asymptotic behavior of the Fourier coefficients near a O(4) transition is also shown.
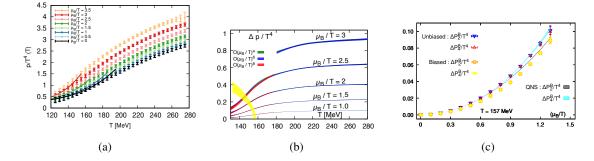
Figure 18: Fig. 18(a) from [66]: The pressure as function of T at different values of μ_B/T compared to the HRG prediction. Fig. 18(b) from [67]: Pressure versus temperature for several values of the baryon chemical potential $\hat{m u}_B \equiv \mu_B/T$ as obtained in different orders of the Taylor series. The yellow bands highlight the variation of $\Delta p/T^4$ with μ_B/T at $T_c(\mu_B/T)$. Fig. 18(c) from [68]: Pressure versus μ_B/T at $T = 157$ MeV.

It has been recently shown [65] that valuable information on the QCD phase diagram can come from calculations of the Fourier coefficients of the net-baryon number density. Their asymptotics at large frequencies is, indeed, governed by singularity structure of the QCD partition function in the complex chemical potential plane, hence encoding information on phase transitions. Their characteristic behavior is also reflected in the baryon number fluctuations that can be reconstructed from the Fourier coefficients. Preliminary lattice results for these Fourier coefficients as a function of a purely imaginary chemical potential have been obtained [63] on HISQ $N_f = 2+1$ gauge configuration ensembles at physical quark masses and nonzero imaginary chemical potential. Sensitivity to the chiral O(4) transition was only found in a narrow temperature interval $T \in [180, 185]$ MeV, below which the exponential suppression associated with the real part of the LYE predominates given the present quadrature method and quark masses.

4.3 Equation of State

The QCD Equation of State (EoS) gives a complete description of equilibrium QCD in terms of relations between thermodynamic observables such as the pressure, the energy density or the entropy density. The phenomenological relevance of the EoS ranges from heavy-ion physics to astrophysics and cosmology.

At nonzero μ_B, due to the sign problem, the EoS is extracted mostly using reweighting or (resummed) Taylor expansion approaches and there has been substantial progress, recently, in such calculations of the EoS. Taylor coefficients of the pressure in the baryon chemical potential are now known for different fermion discretizations up to fourth order, including continuum extrapolations, and up to eighth order at finite lattice spacing. Moreover, several resummation schemes for the Taylor expansion with (empirically observed) better convergence properties have been proposed.

There were several contributions at this year's lattice conference reporting progress in these directions [68, 69] and results are published in several papers [66, 70–74]. In Fig. 18 a collection of figures with results for the pressure in different setups is put together, but the interested reader is referred to the specific references for all the details.
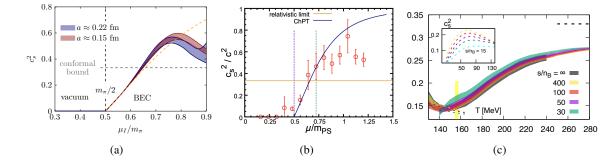
(a)   (b)   (c)

Figure 20: Fig. 20(a) from Ref. [77]: Isentropic c_s^2 at $T = 0$. Also shown are the conformal bound (dashed gray line) and the chiral perturbation theory result (dashed yellow line). Fig. 20(b) from Ref. [78]: c_s^2/c^2 as a function of μ/m_{PS}. Also shown are the conformal bound $c_s^2/c^2 = 1/3$ (orange line) and the chiral perturbation theory result (blue line). Fig. 20(a) from Ref. [67]: c_s^2 in strangeness-neutral, isospin-symmetric matter versus T for several values of s/n_B. The limit $s/n_B = \infty$ corresponds to the case of vanishing chemical potentials. Dashed lines at low T (high T) indicate QMHRG2020 model calculations (the non-interacting quark-gluon gas results). In the inset HRG model results at lower T are shown. The yellow band indicates T_c.

An effort was also made [75] to judge the reliability of different approximation schemes by comparing them with direct nonzero chemical potential results for $\mu_B/T \in [0 - 3]$ using reweighting techniques free from an overlap problem [76] (see Fig. 19).

Finally, results of the QCD phase diagram and EoS with relatively light pions ($\lesssim 480$ MeV) in the $T - \mu_B$ plane have been obtained [56] via complex Langevin simulations covering a baryon number density range of up to ~ 15 times the nuclear sat-

Figure 19: The density $\hat{n}_L$ as a function of the temperature T for $\mu_B/T = 3$ for the ordinary Taylor expansion (bottom) and the resummation schemes based on "shiftings" (top).

uration density $n_0 \simeq 0.16$ fm^{-3} at $T \sim 50$ MeV and up to $\sim 20 n_0$ at $T \sim 200$ MeV. At low T remnants of the Silver Blaze phenomenon were observed, where the quark number density vanishes at $T = 0$ for $\mu < m_N/3$ and the pressure EoS was found to become stiffer for lower T.

4.4 Speed of sound

Another interesting observable related to the EoS is the speed of sound c_s, which is very relevant to astrophysics, namely as a proxy to distinguish stars with and without deconfined quark matter cores. The isentropic speed of sound, i.e., the speed of a sound wave travelling isentropically through the plasma, is defined as a derivative of the pressure density w.r.t. the energy density in the

direction of isentropic trajectories in phase space, i.e., for QCD at generic nonzero quark chemical potentials in the direction where

$$\frac{s}{n_q} = \text{const} \quad \forall \text{ flavors } q \qquad (q = u,\, d,\, s \text{ for } N_f = 2 + 1)\,. \qquad (5)$$

Recently, the observation of an EoS in QCD at small temperatures (and nonzero isospin density) with a speed of sound not only beyond the conformal bound, but even up to $c_s^2 \gtrsim 0.5$ was reported in Refs. [77, 79] (see Fig. 20(a)). This observation matches the experimental constraints, according to recent studies, that favour a stiff EoS with a speed of sound that exceeds the conformal limit. Moreover, the finding of $c_s^2 > 1/3$, as well as the development of a peak in isospin-QCD is in good agreement with recent results obtained in two-color QCD[2] [78, 82] (see Fig. 20(b)). Yet another determination of the speed of sound is to be found in Refs. [67, 83] where the isentropic speed of sound is calculated on the lines of constant $s/n_{\rm B}$, in a strangeness neutral medium at non-vanishing net baryon-number density with fixed $n_{\rm Q}/n_{\rm B}$, and for $T \in [125 - 180]$ MeV. It is shown that the minimum in c_s^2, present at zero baryon chemical potential, for $s/n_{\rm B} > 100$, at temperatures close to the pseudo-critical line, will disappear at smaller values of $s/n_{\rm B}$, *i.e.*, for large $n_{\rm B}$ close to $T_{\rm c}$.

4.5 Properties of dense QGP

A study of the electromagnetic conductivity in dense quark-gluon plasma obtained within lattice simulations with $N_{\rm f} = 2 + 1$ stout improved rooted staggered quarks at the physical point and the tree-level Symanzik improved gauge action was also reported at this conference. Simulations were performed at imaginary chemical potential. The Tikhonov regularization method as well as the modified Backus-Gilbert method [84] were employed to reconstruct electromagnetic conductivity from current-current correlators, computing the convolution of the spectral density with the target function. This study indicates that electromagnetic conductivity of the QGP rapidly grows with the real baryon density, and the conductivity is studied also in presence of strong magnetic fields. Results are however, to the best of our knowledge, yet unpublished.

The long-distance behavior of spatial correlation functions is influenced by the way the finite temporal extents of the Euclidean lattice, through which a nonzero temperature is implemented, acts, like a finite volume effect, on spatial quark and anti-quark propagators. The exponential decay of spatial correlation functions at large distances defines screening masses, which differ from the pole masses at zero temperature, and approach multiples of πT at high T, signaling the propagation of free quark quasi-particles in the thermal medium. Progress towards the determination, using Taylor expansion, of the dependence on a nonzero isoscalar chemical potential of screening masses in QCD (specifically that of the pseudoscalar meson) is reported in Ref. [85] where both the free and the interacting theory are discussed, and the screening mass is allowed to take complex values motivated by the free theory analytical expression for the screening correlator showing an oscillatory behavior that suggests a complex screening mass.

---

[2]Besides progress on the EoS and speed of sound, in the context of two-flavor and two-color QCD also the modifications of hadron masses at finite quark chemical potential have been investigated [80, 81] within a linear sigma model based on approximate Pauli-Gursey SU(4) symmetry.

4.6 The cold and dense regime

The phase structure of QCD at a few times nuclear-matter density and low to moderate temperatures is relevant for neutron stars and neutron-star mergers as well as for heavy-ion collisions at moderate collision energies.

The Hamiltonian formulation of lattice QCD with staggered fermions in the strong coupling limit allows for Quantum Monte Carlo (QMC) simulations at non-zero baryon density. Ref. [86] reports on an extension to the Hamiltonian formulation of strong coupling lattice QCD from $N_f = 1$ to $N_f = 2$, aiming at mapping out the enlarged phase diagram in the strong coupling regime in the μ_B-μ_I-T-space, as well as on progress on the implementation of the QMC simulations for the $N_f = 2$ case, in which simulations are doable both for nonzero baryon and for nonzero isospin chemical potential. In the strong coupling limit and for $N_f = 1$, the dual formulation with staggered quarks is well established and has been used [87] to study the quark mass dependence of the baryon mass and the nuclear transition allowing for a quantification of the nuclear interaction that tends to zero when the quark mass is large and is found to be in agreement, at large quark masses, with the 3-dim. Polyakov loop effective theory based on hopping parameter expansion.

Polyakov loop effective theories obtained by integrating out the spatial gauge links in a strong-coupling and hopping parameter expansion give access to the cold & dense regime of QCD, in the heavy quark mass regime. However, in this context, a new set of couplings appear whose expressions in terms of the gauge coupling and N_τ are only known from strong-coupling expansions. As a way to determine the temperature dependence of the effective couplings, using the finite-cluster method, high-order expressions for correlators of Polyakov loops in the effective theory are computed [88] and mapped to those in full lattice QCD. Moreover, while the evaluation of Polyakov loop effective theories is complicated by the appearance of long-range and multipoint interaction terms appearing beyond leading order in the expansion parameters, for theories with these type of interactions results from mean field approximations can be expected to be reliable. In Ref. [89] the mean field framework improved via a resummation of fluctuations is applied to the critical endpoint of the deconfinement transition both in the pure gauge limit and with three flavors of heavy quarks. This treatment has also been used to investigate the phase diagram at non-zero baryon and isospin chemical potential with results reported in Ref. [90].

Several QCD-inspired effective models predict for the cold and dense regime, in mean-field approximation, the existence of an inhomogeneous phase. In an inhomogeneous chiral phase both chiral symmetry and translational symmetry are broken by a non-zero, spatially oscillating, chiral condensate. While most of the existing model calculations neglect bosonic quantum fluctuations by being restricted to the mean-field approximation, evidence that inhomogeneous regimes also exist in full QFTs comes from lattice Monte-Carlo simulations of the $1 + 1$-dimensional Gross-Neveu model [91]. This observation motivated further investigations of $3 + 1$-dimensional models that are closer to QCD. However, for the $3 + 1$-dimensional Nambu-Jona-Lasinio (NJL) model in the mean field-approximation, upon employing five different regularization schemes (three of which were lattice regularization schemes) drastically different results were obtained for the inhomogeneous phase.Based on this evidence, Ref. [92] suggests that inhomogeneous phases in the 3+1-dimensional NJL model are rather artifacts of the regularization. At the same time, a variety of four-fermion and Yukawa models in $2 + 1$ dimensions at zero and non-zero temperature and chemical potentials

have been investigated [93] employing the mean-field approximation. In this case, no indication for an inhomogeneous phase was found in any of the models, which are shown to only feature homogeneous phases that are stable against inhomogeneous perturbations. Finally, simulations of the Gross-Neveu model in 2 + 1 dimensions are being performed in a constant and homogeneous magnetic field using one reducible flavor of overlap fermions. Whether the inclusion of a constant magnetic field might bring back inhomogeneities remains an open question, but results on the phase diagram have been obtained [94].

5. Conclusions

Despite the fact that mapping out completely the phase diagram of QCD is a formidable problem, there has been a lot of efforts within the lattice community to impose more stringent constraints in the region where lattice simulations are feasible and trustworthy. This quest is fueled by the will to understand phenomenologically driven questions regarding the existence and location of the elusive critical point, new phases of nuclear matter under extreme conditions but also theoretical questions regarding for example the nature of the chiral phase transition in the chiral limit. Final answers, have not been given to any of those queries. However, the lattice community is making constant progress in all the aforementioned fronts despite being hindered by the sign problem. In this proceeding, we gave the most recent update in a vast number of subjects which are covered by the large umbrella of thermodynamics of QCD. From what we presented, it is clear that there is a bright future waiting for our community since despite our progress we are only in the very beginning of the systematic study of the QCD phase diagram, but with the algorithmic developments throughout the years as well as with the fact that we are entering the era of exascale computing we are very optimistic and excited for the years to come.

6. Acknowledgments

References

[1] NA61/SHINE collaboration, *Looking for the Phase Transition—Recent NA61/SHINE Results*, *Universe* **4** (2018) 52 [1801.06919].

[2] G. Aarts et al., *Phase Transitions in Particle Physics – Results and Perspectives from Lattice Quantum Chromo-Dynamics*, 1, 2023 [2301.04382].

[3] R.A. Vig, S. Borsanyi, Z. Fodor, D. Godzieba, R. Kara, P. Parotto et al., *Topological features of the deconfinement transition in the SU(3) Yang-Mills theory*, *PoS* **LATTICE2022** (2023) 194.

[4] T.G. Kovacs, *Topology and the Dirac Spectrum in Hot QCD*, *PoS* **LATTICE2022** (2023) 180 [2212.05824].

[5] F. Cuteri, O. Philipsen and A. Sciarra, *On the order of the QCD chiral phase transition for different numbers of quark flavours*, *JHEP* **11** (2021) 141 [2107.12739].

[6] R.F. Basta, B.B. Brandt, F. Cuteri, G. Endrődi and A. Francis, *QCD thermodynamics with stabilized Wilson fermions*, *PoS* **LATTICE2022** (2022) 277 [2212.09916].

[7] Y. Zhang, Y. Aoki, S. Hashimoto, I. Kanamori, T. Kaneko and Y. Nakamura, *Finite temperature QCD phase transition with 3 flavors of Möbius domain wall fermions*, *PoS* **LATTICE2022** (2022) 197 [2212.10021].

[8] M. Cardinali, M. D'Elia, F. Garosi and M. Giordano, *Localization properties of Dirac modes at the Roberge-Weiss phase transition*, *Phys. Rev. D* **105** (2022) 014506 [2110.10029].

[9] V.G. Bornyakov, N.V. Gerasimeniuk, V.A. Goy, A.A. Korneev, A.V. Molochkov, A. Nakamura et al., *Numerical study of the Roberge-Weiss transition*, *Phys. Rev. D* **107** (2023) 014508 [2203.06159].

[10] F. Cuteri, J. Goswami, F. Karsch, A. Lahiri, M. Neumann, O. Philipsen et al., *Toward the chiral phase transition in the Roberge-Weiss plane*, *Phys. Rev. D* **106** (2022) 014510 [2205.12707].

[11] B.B. Brandt, A. Chabane, V. Chelnokov, F. Cuteri, G. Endrődi and C. Winterowd, *The light Roberge-Weiss tricritical endpoint at imaginary isospin and baryon chemical potential*, 2207.10117.

[12] A. D'Ambrosio, O. Philipsen and R. Kaiser, *The chiral phase transition at non-zero imaginary baryon chemical potential for different numbers of quark flavours*, *PoS* **LATTICE2022** (2022) 172 [2212.03655].

[13] A. Kiyohara, M. Kitazawa, S. Ejiri and K. Kanaya, *Finite-size scaling around the critical point in the heavy quark region of QCD*, *Phys. Rev. D* **104** (2021) 114509 [2108.00118].

[14] S. Borsanyi, K. R., Z. Fodor, D.A. Godzieba, P. Parotto and D. Sexty, *Precision study of the continuum SU(3) Yang-Mills theory: How to use parallel tempering to improve on supercritical slowing down for first order phase transitions*, *Phys. Rev. D* **105** (2022) 074513 [2202.05234].

[15] K. Kanaya, R. Ashikawa, S. Ejiri, M. Kitazawa, H. Suzuki and N. Wakabayashi, *Phase structure and critical point in heavy-quark QCD at finite temperature*, *PoS* **LATTICE2022** (2022) 177 [2211.08631].

[16] R. Kaiser and O. Philipsen, *Progress on the QCD Deconfinement Critical Point for $N_f = 2$ Staggered Fermions*, *PoS* **LATTICE2022** (2023) 175 [2212.14461].

[17] R. Kara, S. Borsanyi, Z. Fodor, D.A. Godzieba, P. Parotto and D. Sexty, *Parallel tempering algorithm applied to the deconfinement transition of quenched QCD*, *PoS* **LATTICE2022** (2023) 178 [2212.10155].

[18] G. Aarts et al., *Properties of the QCD thermal transition with Nf=2+1 flavors of Wilson quark*, *Phys. Rev. D* **105** (2022) 034504 [2007.04188].

[19] G. Aarts, C. Allton, R. Bignell, T.J. Burns, S.C. García-Mascaraque, S. Hands et al., *Open charm mesons at nonzero temperature: results in the hadronic phase from lattice QCD*, 2209.14681.

[20] C. Allton et al., *Recent Results from the FASTSUM Collaboration*, *PoS* **LATTICE2022** (2022) 198 [2301.10282].

[21] R. Bignell, G. Aarts, C. Allton, M.N. Anwar, T.J. Burns and B. Jäger, *Charm baryons at finite temperature on anisotropic lattices*, *PoS* **LATTICE2022** (2023) 170 [2212.09371].

[22] B. Page, C. Allton and S. Kim, *Novel Bottomonium Results*, *PoS* **LATTICE2022** (2022) 187 [2212.12016].

[23] T. Spriggs, C. Allton, T. Burns and S. Kim, *New results for thermal interquark bottomonium potentials using NRQCD from the HAL QCD method*, *PoS* **LATTICE2022** (2023) 192 [2301.03320].

[24] HotQCD collaboration, *Static quark-antiquark interactions at nonzero temperature from lattice QCD*, *Phys. Rev. D* **105** (2022) 054513 [2110.11659].

[25] G. Parkar, O. Kaczmarek, R. Larsen, S. Mukherjee, P. Petreczky, A. Rothkopf et al., *Complex potential at T > 0 from fine lattices*, *PoS* **LATTICE2022** (2023) 188.

[26] S. Ali, D. Bala, O. Kaczmarek, H.-T. Shu and T. Ueding, *Study of charm and beauty in QGP from unquenched lattice QCD*, *PoS* **LATTICE2022** (2022) 166 [2212.12357].

[27] B.B. Brandt, A. Francis, H.B. Meyer and D. Robaina, *Pion quasiparticle in the low-temperature phase of QCD*, *Phys. Rev. D* **92** (2015) 094510 [1506.05732].

[28] M. Cè, T. Harris, A. Krasniqi, H. Meyer, S. Ruhl and C. Török, *A (2 + 1)-flavor lattice study of the pion quasiparticle in the thermal hadronic phase at physical quark masses*, *PoS* **Lattice2022** (2022) 0181.

[29] M. Cè, T. Harris, A. Krasniqi, H.B. Meyer and C. Török, *Aspects of chiral symmetry in QCD at T = 128 MeV*, 2211.15558.

[30] M. Dalla Brida, L. Giusti, T. Harris, D. Laudicina and M. Pepe, *Non-perturbative thermal QCD at all temperatures: the case of mesonic screening masses*, *JHEP* **04** (2022) 034 [2112.05427].

[31] A. Bazavov et al., *Meson screening masses in (2+1)-flavor QCD*, *Phys. Rev. D* **100** (2019) 094510 [1908.09552].

[32] O. Philipsen, L.Y. Glozman, P. Lowdon and R.D. Pisarski, *On chiral spin symmetry and the QCD phase diagram*, *PoS* **LATTICE2022** (2022) 189 [2211.11628].

[33] C. Rohrhofer, Y. Aoki, L.Y. Glozman and S. Hashimoto, *Chiral-spin symmetry of the meson spectral function above T_c*, *Phys. Lett. B* **802** (2020) 135245 [1909.00927].

[34] L.Y. Glozman, O. Philipsen and R.D. Pisarski, *Chiral spin symmetry and the QCD phase diagram*, *Eur. Phys. J. A* **58** (2022) 247 [2204.05083].

[35] P. Lowdon and O. Philipsen, *Pion spectral properties above the chiral crossover of QCD*, *JHEP* **10** (2022) 161 [2207.14718].

[36] M. Cè, T. Harris, A. Krasniqi, H.B. Meyer and C. Török, *Photon emissivity of the quark-gluon plasma: A lattice QCD analysis of the transverse channel*, *Phys. Rev. D* **106** (2022) 054501 [2205.02821].

[37] D. Bala, S. Ali, A. Francis, G. Jackson, O. Kaczmarek and T. Ueding, *Photon production rate from Transverse-Longitudinal (T − L) mesonic correlator on the lattice*, *PoS* **LATTICE2022** (2022) 169 [2212.11509].

[38] C. Török, M. Cè, T. Harris, A. Krasniqi, H.B. Meyer and S. Ruhl, *Estimation of the photon production rate using imaginary momentum correlators*, *PoS* **LATTICE2022** (2022) 193 [2212.05622].

[39] S. Caron-Huot and G.D. Moore, *Heavy quark diffusion in qcd and $\mathcal{N}$ = 4 sym at next-to-leading order*, *Journal of High Energy Physics* **2008** (2008) 081.

[40] D. Banerjee, S. Datta, R. Gavai and P. Majumdar, *Heavy quark momentum diffusion coefficient from lattice qcd*, *Phys. Rev. D* **85** (2012) 014510.

[41] A. Francis, O. Kaczmarek, M. Laine, T. Neuhaus and H. Ohno, *Nonperturbative estimate of the heavy quark momentum diffusion coefficient*, *Phys. Rev. D* **92** (2015) 116003.

[42] L. Altenkort, A.M. Eller, O. Kaczmarek, L. Mazur, G.D. Moore and H.-T. Shu, *Heavy quark momentum diffusion from the lattice using gradient flow*, *Phys. Rev. D* **103** (2021) 014511.

[43] N. Brambilla, V. Leino, P. Petreczky, A. Vairo, T. Collaboration et al., *Lattice qcd constraints on the heavy quark diffusion coefficient*, *Physical Review D* **102** (2020) 074503.

[44] D. Banerjee, S. Datta and M. Laine, *Lattice study of a magnetic contribution to heavy quark momentum diffusion*, *JHEP* **08** (2022) 128 [2204.14075].

[45] D. Banerjee, R. Gavai, S. Datta and P. Majumdar, *Temperature dependence of the static quark diffusion coefficient*, 2206.15471.

[46] TUMQCD collaboration, *Heavy quark diffusion coefficient with gradient flow*, 2206.02861.

[47] V. Leino, N. Brambilla, J. Mayer-Steudte and P. Petreczky, *Heavy quark diffusion coefficient with gradient flow*, *PoS* **LATTICE2022** (2023) 183 [2212.10941].

[48] M. D'Elia, L. Maio, F. Sanfilippo and A. Stanzione, *Phase diagram of QCD in a magnetic background*, *Phys. Rev. D* **105** (2022) 034511 [2111.11237].

[49] G. Endrodi, *Critical point in the QCD phase diagram for extremely strong background magnetic fields*, *JHEP* **07** (2015) 173 [1504.08280].

[50] M. D'Elia, L. Maio, F. Sanfilippo and A. Stanzione, *Phase diagram of QCD in strong background magnetic field*, *PoS* **ICHEP2022** (2022) 414 [2211.12166].

[51] A.D. Marques Valois, B. Brandt, F. Cuteri, G. Endrodi and G. Marko, *Lattice QCD with an inhomogeneous magnetic field background*, *PoS* **LATTICE2021** (2022) 083 [2111.13100].

[52] E.G. Velasco, B.B. Brandt, F. Cuteri, G. Endrődi and G. Markó, *Anomalous transport phenomena on the lattice*, *PoS* **LATTICE2022** (2023) 173 [2212.02148].

[53] B. Brandt, F. Cuteri, G. Endrődi, J.J.H. Hernández and G. Markó, *QCD topology with electromagnetic fields and the axion-photon coupling*, *PoS* **LATTICE2022** (2022) 174 [2212.03385].

[54] V.V. Braguta, A. Kotov, A. Roenko and D. Sychev, *Thermal phase transitions in rotating QCD with dynamical quarks*, *PoS* **LATTICE2022** (2023) 190 [2212.03224].

[55] Z. Tulipant, M. Giordano, K. Kapas, S.D. Katz and A. Pasztor, *Exponential improvement of the sign problem via contour deformations in the 2+1D XY model at non-zero density*, *Phys. Rev. D* **106** (2022) 054512 [2202.07561].

[56] F. Attanasio, B. Jäger and F.P.G. Ziegler, *QCD equation of state via the complex Langevin method*, 2203.13144.

[57] M.W. Hansen and D. Sexty, *Complex Langevin boundary terms in full QCD*, *PoS* **LATTICE2022** (2022) 163 [2212.12029].

[58] P. Dimopoulos, L. Dini, F. Di Renzo, J. Goswami, G. Nicotra, C. Schmidt et al., *Contribution to understanding the phase structure of strong interaction matter: Lee-Yang edge singularities from lattice QCD*, *Phys. Rev. D* **105** (2022) 034513 [2110.15933].

[59] F. Di Renzo and S. Singh, *Multi-point Padè for the study of phase transitions: from the Ising model to lattice QCD*, *PoS* **LATTICE2022** (2023) 148 [2301.03528].

[60] K. Zambello, D.A. Clarke, P. Dimopoulos, F. Di Renzo, J. Goswami, G. Nicotra et al., *Determination of Lee-Yang edge singularities in QCD by rational approximations*, *PoS* **LATTICE2022** (2023) 164 [2301.03952].

[61] B.B. Brandt, V. Chelnokov, F. Cuteri and G. Endrődi, *Pion condensation at lower than physical quark masses*, *PoS* **LATTICE2022** (2023) 146 [2301.08607].

[62] S. Sharma, *Charm fluctuations in (2+1)-flavor QCD at high temperature*, *PoS* **LATTICE2022** (2022) 191 [2212.11148].

[63] C. Schmidt, *Fourier coefficients of the net-baryon number density*, *PoS* **LATTICE2022** (2023) 159 [2301.04978].

[64] A. Bazavov et al., *The melting and abundance of open charm hadrons*, *Phys. Lett. B* **737** (2014) 210 [1404.4043].

[65] G.A. Almasi, B. Friman, K. Morita, P.M. Lo and K. Redlich, *Fourier coefficients of the net-baryon number density and chiral criticality*, *Phys. Rev. D* **100** (2019) 016016 [1805.04441].

[66] S. Borsanyi, J.N. Guenther, R. Kara, Z. Fodor, P. Parotto, A. Pasztor et al., *Resummed lattice QCD equation of state at finite baryon density: Strangeness neutrality and beyond*, *Phys. Rev. D* **105** (2022) 114504 [2202.05574].

[67] D. Bollweg, D.A. Clarke, J. Goswami, O. Kaczmarek, F. Karsch, S. Mukherjee et al., *Equation of state and speed of sound of (2+1)-flavor QCD in strangeness-neutral matter at non-vanishing net baryon-number density*, 2212.09043.

[68] S. Mitra, P. Hegde and C. Schmidt, *A new way to resum Lattice QCD equation of state at finite chemical potential*, *PoS* **LATTICE2022** (2023) 153 [2209.07241].

[69] HotQCD collaboration, *The isentropic equation of state of (2+1)-flavor QCD: An update based on high precision Taylor expansion and Pade-resummed expansion at finite chemical potentials*, *PoS* **LATTICE2022** (2023) 149 [2212.10016].

[70] HotQCD collaboration, *Taylor expansions and Padé approximants for cumulants of conserved charge fluctuations at nonvanishing chemical potentials*, *Phys. Rev. D* **105** (2022) 074511 [2202.09184].

[71] S. Borsányi, Z. Fodor, J.N. Guenther, R. Kara, S.D. Katz, P. Parotto et al., *Lattice QCD equation of state at finite chemical potential from an alternative expansion scheme*, *Phys. Rev. Lett.* **126** (2021) 232001 [2102.06660].

[72] S. Mitra and P. Hegde, *New formalism for unbiased exponential resummation of Lattice QCD Taylor series at finite baryon chemical potential*, 2209.11937.

[73] S. Mitra, P. Hegde and C. Schmidt, *New way to resum the lattice QCD Taylor series equation of state at finite chemical potential*, *Phys. Rev. D* **106** (2022) 034504 [2205.08517].

[74] S. Mondal, S. Mukherjee and P. Hegde, *Lattice QCD Equation of State for Nonvanishing Chemical Potential by Resumming Taylor Expansions*, *Phys. Rev. Lett.* **128** (2022) 022001 [2106.03165].

[75] S. Borsanyi, Z. Fodor, M. Giordano, J.N. Guenther, S.D. Katz, A. Pasztor et al., *Equation of state of a hot-and-dense quark gluon plasma: lattice simulations at real μ_B vs. extrapolations*, 2208.05398.

[76] M. Giordano, K. Kapas, S.D. Katz, D. Nogradi and A. Pasztor, *New approach to lattice QCD at finite density; results for the critical end point on coarse lattices*, *JHEP* **05** (2020) 088 [2004.10800].

[77] B.B. Brandt, F. Cuteri and G. Endrodi, *Equation of state and speed of sound of isospin-asymmetric QCD on the lattice*, 2212.14016.

[78] E. Itou and K. Iida, *Bump of sound velocity in dense 2-color QCD*, *PoS* **LATTICE2022** (2023) 151 [2210.14385].

[79] B.B. Brandt, F. Cuteri and G. Endrödi, *Equation of state and Taylor expansions at nonzero isospin chemical potential*, *PoS* **LATTICE2022** (2023) 144 [2212.01431].

[80] K. Murakami, D. Suenaga, K. Iida and E. Itou, *Measurement of hadron masses in 2-color finite density QCD*, *PoS* **LATTICE2022** (2023) 154 [2211.13472].

[81] D. Suenaga, K. Murakami, E. Itou and K. Iida, *Probing hadron mass spectrum in dense two-color QCD with linear sigma model*, 2211.01789.

[82] K. Iida and E. Itou, *Velocity of sound beyond the high-density relativistic limit from lattice simulation of dense two-color QCD*, *PTEP* **2022** (2022) 111B01 [2207.01253].

[83] D.A. Clarke, *Isothermal and isentropic speed of sound in (2+1)-flavor QCD at non-zero baryon chemical potential*, *PoS* **LATTICE2022** (2023) 147 [2212.10009].

[84] M. Hansen, A. Lupo and N. Tantalo, *Extraction of spectral densities from lattice correlators*, *Phys. Rev. D* **99** (2019) 094508 [1903.06476].

[85] R. Thakkar and P. Hegde, *Meson screening mass at finite chemical potential*, *PoS* **LATTICE2022** (2023) 160 [2211.10072].

[86] W. Unger and P. Pattanaik, *Towards Quantum Monte Carlo Simulations at non-zero Baryon and Isospin Density in the Strong Coupling Regime*, *PoS* **LATTICE2022** (2023) 162 [2212.11328].

[87] P. Pattanaik, W. Unger and J. Kim, *Nuclear Transition in the Strong Coupling Limit.*, *PoS* **LATTICE2022** (2023) 158 [2212.03118].

[88] C. Winterowd, O. Philipsen and J. Scheunert, *Non-perturbative determination of couplings in Polyakov loop effective theories*, *PoS* **LATTICE2022** (2023) 196.

[89] C. Konrad, O. Philipsen and J. Scheunert, *Mean field approximation for effective theories of lattice QCD*, *PoS* **LATTICE2022** (2023) 179 [2212.04417].

[90] A. Chabane and O. Philipsen, *Towards the phase diagram of cold and dense heavy QCD*, *PoS* **LATTICE2022** (2023) 145 [2212.09591].

[91] J. Lenz, L. Pannullo, M. Wagner, B. Wellegehausen and A. Wipf, *Inhomogeneous phases in the Gross-Neveu model in 1+1 dimensions at finite number of flavors*, *Phys. Rev. D* **101** (2020) 094512 [2004.00295].

[92] L. Pannullo, M. Wagner and M. Winstel, *Inhomogeneous phases in the 3+1-dimensional Nambu-Jona-Lasinio model and their dependence on the regularization scheme*, *PoS* **LATTICE2022** (2023) 156 [2212.05783].

[93] M. Winstel and L. Pannullo, *Stability of homogeneous chiral phases against inhomogeneous perturbations in 2+1 dimensions*, *PoS* **LATTICE2022** (2022) 195 [2211.04414].

[94] M. Mandl, J.J. Lenz and A. Wipf, *Magnetic catalysis in the 1-flavor Gross-Neveu model in 2 + 1 dimensions*, *PoS* **LATTICE2022** (2022) 152 [2211.10333].